ARTICLES

Trajectory Studies of S_N2 Nucleophilic Substitution. 6. Translational Activation of the $Cl^- + CH_3Cl$ Reaction

David J. Mann and William L. Hase*

Department of Chemistry, Wayne State University, Detroit, Michigan 48202-3489

Received: March 4, 1998; In Final Form: June 1, 1998

Classical trajectory simulations are used to study the translational activation of the $Cl^- + CH_3Cl$ S_N2 reaction at energies in the range 20−80 kcal/mol. The trajectories are calculated on the PES3 analytic potential energy surface. The shape of the reactive cross section versus relative translational energy E_{rel} and the translational threshold of 18 kcal/mol are both similar to recent experimental results [*J. Phys. Chem. A* **1997**, *101*, 5969]. The reactive trajectories are direct, with negligible trapping in the ion−dipole complexes. The product energy is primarily partitioned to relative translation with small and similar amounts of energy partitioned to vibration and rotation. The velocity scattering angle distribution suggests backward scattering and a rebound mechanism for translational activation at low E_{rel}, with increasing importance of forward scattering and a stripping mechanism as E_{rel} is increased. An analysis of angular momenta terms and their correlations shows that the total angular momentum is well-approximated by the initial orbital angular momentum, which is strongly correlated with the final orbital angular momentum. The decrease in the reactive cross section with CD_3Cl isotopic substitution is consistent with the experiments. The principal difference between the trajectories and experiments is the order of magnitude larger cross sections found from the trajectories. No pronounced inadequacies in the PES3 potential energy surface are evident from comparisons with MP2/6-311+G** ab initio calculations.

I. Introduction

Gas-phase S_N2 nucleophilic substitution reactions of the type

$$X^- + CH_3Y \rightarrow XCH_3 + Y^- \qquad (1)$$

have been the focus of many recent experimental[1] and theoretical[2] studies. One of the reasons for the interest in these reactions is the range of possible reaction dynamics arising from the potential energy minima for the pre- and postreaction ion−dipole complexes X^-- - -CH_3Y and XCH_3- - -Y^-.[3] Both theory and experiment indicate that important kinetic and dynamic properties of these reactions cannot be modeled by the transition state, Rice−Ramsperger−Kassel−Marcus (RRKM), and phase space theories.[3,4] If the S_N2 reactive system becomes trapped in the ion−dipole potential energy minima, the form of the reagent energy, whether vibrational or translational, should have no effect on either the reaction probability or the product energy partitioning, if angular momentum is properly treated. Contrary to such a model, trajectory calculations[2a,e,3−5] for the $Cl^- + CH_3Cl$ and $Cl^- + CH_3Br$ S_N2 systems and experiments[1a,d] for the $Cl^- + CH_3Br$ S_N2 system suggest that vibrational excitation of the rupturing C−Y bond is particularly effective in promoting reaction and that energy is partitioned nonstatistically to the reaction products.

There have been several experimental studies[1i,k] of the symmetric S_N2 reaction

$$Cl^- + CH_3Cl \rightarrow ClCH_3 + Cl^- \qquad (2)$$

In pioneering work by Bierbaum and co-workers,[1k] the rate constant for reaction 2 was measured at 300 K and as a function of center-of-mass collision energy (i.e., translational activation). Deconvolution of the latter set of experiments yielded an apparent threshold of 45 kcal/mol, which was attributed to a high-energy mechanism involving anionic attack at the chlorine atom of chloromethane. Such a threshold is consistent with ab initio stationary point calculations[2j,k] but less consistent with ab initio reaction path calculations.[1i] In recent experiments, Ervin and co-workers[1i] have studied the translational activation of reaction 2 with finer resolution of the collision energy. They find a translational threshold for this reaction of 11 ± 4 kcal/mol, which is appreciably higher than the value of 2.5−3.0 kcal/mol determined from ab initio calculations and fits of statistical theories to the 300 K thermal rate constant. A translational threshold larger than the potential energy barrier is consistent with trajectory calculations,[3−5] which indicate the reaction is promoted by CH_3−Cl stretch vibrational excitation. The translational threshold measured by Ervin and co-workers is substantially lower than the threshold proposed for the anionic attack mechanism.

In the work reported here trajectory calculations are used to simulate the experiments of Ervin and co-workers for reaction 2. The calculations are performed using the analytic potential energy surface PES3, which is a modification of PES2/R,[6] developed previously for reaction 2 from experimental and ab initio data. The information obtained from the trajectories are the reaction cross section, product energy and velocity scattering angle distributions, and angular momenta correlations as a

S1089-5639(98)01359-0 CCC: $15.00
Published on Web 07/15/1998

TABLE 1: Stationary Point Geometries and Energies for PES3[a]

	reactants $Cl^- + CH_3Cl$	complex Cl^-- - -CH_3Cl	central barrier [Cl- -CH_3- -Cl]$^-$
r_a	∞	3.322	2.3860
r_b	1.7846	1.824	2.3860
r_{HC}	1.0778	1.0727	1.0613
ϕ_b	108.453	108.240	90.0
θ	110.470	110.673	120.0
energy[b]	0	−10.278	3.533

[a] Distances are in angstroms and angles in degrees. r_a and r_b are the C−Cl_a and C−Cl_b distances for Cl_a^-- - -CH_3Cl_b. r_{HC} is the HC distance, ϕ_b is H−C−Cl_b angle, and θ is the H−C−H angle. [b] Potential energy is in kcal/mol.

TABLE 2: Stationary Point Harmonic Vibrational Frequencies for PES3[a]

vib mode[b]	reactants $Cl^- + CH_3Cl$	complex Cl^-- - -CH_3Cl	central barrier [Cl- -CH_3- -Cl]$^-$
A_1, C−H str	3037	3104	3218
A_1, CH_3 def	1445	1434	1041
A_1, C−Cl_b str	739	678	196
A_1, C−Cl_a str		107	398i
E, C−H str	3166	3242	3419
E, CH_3 def	1438	1432	1330
E, CH_3 rock	984	1003	1025
E, Cl_a bend		71	162

[a] Frequencies are in cm^{-1}. [b] Cl_a and Cl_b are identified by Cl_a^-- - -CH_3Cl_b.

function of reactant relative translational energy. It is hoped that this study will provide a deeper understanding of the dynamics of reaction 2 and other gas-phase S_N2 reactions.

II. PES3 Analytic Potential Energy Function

An approximation made in developing the potential function PES2/R for reaction 2 is that the HC stretching potential does not change for different regions of the potential energy surface. In contrast, ab initio calculations[2d,6a] show that the HC stretching potential stiffens in proceeding from the $Cl^- + CH_3Cl$ reactants to the Cl^-- - -CH_3Cl complex and then the [Cl- -CH_3- -Cl]$^-$ central barrier. This tightening is manifested by a shorter HC equilibrium bond length r_{HC} and higher HC stretching force constant f_{HC}. These properties are incorporated into PES3 by making both r_{HC} and f_{HC} functions of the *extent of reaction* term $g = g_a = r_a - r_b = |g_b| = |r_b - r_a|$, where r_a and r_b are the two C−Cl distances for $Cl_a^- + CH_3Cl_b$.

Values of r_{HC} for the reactants, complex, and central barrier, determined previously from HF/6-31G* calculations,[6a] are 1.0778, 1.0729, and 1.0613 Å, respectively, and were used to write r_{HC} as a function of g. The form used for $r_{HC}(g)$ is

$$r_{HC}(g) = r_0^{\infty} + (r_0^{\ddagger} - r_0^{\infty})S_r(g) \tag{3}$$

when r_0^{∞} and $r_0^{\ddagger}$ are the "equilibrium" bond lengths for the reactants and central barrier and $S_r(g)$ is the switching function

$$S_r(g) = e^{-c_r g^2} \tag{4}$$

A value for c_r of 0.587 962 097 $Å^{-2}$ was chosen to fit $r_{HC}(g)$ for the complex. (Note that $g = 0$ at the central barrier.)

The value of f_{HC} for the reactants was fit to the experimental[7] harmonic HC stretching frequencies, while values of f_{HC} for the complex and central barrier were fit to "scaled" HF/6-31G* harmonic HC stretching frequencies.[6a] The Morse function parameter β_{HC} was expressed as a function of g by

$$\beta_{HC}(g) = \beta_0^{\infty} + (\beta_0^{\ddagger} - \beta_0^{\infty})S_\beta(g) \tag{5}$$

where the β_{HC} values for the reactants and central barrier are $\beta_0^{\infty} = 1.8670$ and $\beta_0^{\ddagger} = 2.0054$, respectively. The switching function $S_\beta(g)$ is given by

$$S_\beta(g) = e^{-c_\beta g^2} \tag{6}$$

where $c_\beta = 0.503\,819\,015$ $Å^{-2}$ was chosen to fit β_{HC} of 1.9159 $Å^{-1}$ for the complex.

Geometries, energies, and harmonic vibrational frequencies determined from PES3 for the reactants, complex, and central barrier are listed in Tables 1 and 2. The exact location of the complex on the potential energy surface was found by following the negative of the gradient vector. The coordinate driving method was used to find the structure of the central barrier. Experimental, HF/6-31G*, and "scaled" HF/6-31G* geometries, energies, and vibrational frequencies for reaction 2 have been listed and compared previously.

PES3 was not fit to the ab initio transition state and reaction path data[1i,2j,k] for the anionic attack mechanism proposed for reaction 2.[1k] Thus, this pathway is not represented by PES3, and the trajectories calculated for this work cannot be used to study the dynamics of anionic attack of chlorine. An investigation of the dynamics of this mechanism would be of interest in future work.

III. Computational Procedure

The same computational procedure was used for this trajectory study as for previous trajectory studies of gas-phase S_N2 reactions. The trajectories were calculated with the general chemical dynamics computer program VENUS96,[8] by adding PES3 to this computer program. Initial conditions were chosen for a fixed $Cl^- + CH_3Cl$ relative translational energy E_{rel} of 20−80 kcal/mol and a CH_3Cl vibrational/rotational temperature of 300 K. Since the HC stretching and HCH deformation modes are expected to be primarily "spectators" during the reaction[2f] and any leakage of zero-point energy from these modes could have a deleterious effect on the reaction dynamics,[9,10] energy was only added to the two modes most strongly participating in the S_N2 reaction, i.e., the A_1 C−Cl stretch and A_1 CH_3 umbrella modes, in sampling a 300 K Boltzmann distribution energy. Tests were performed to check whether sampling all the modes produced any significant differences than sampling only the CCl stretch and CH_3 umbrella modes. Trajectory calculations showed that both approaches give results that are in statistical agreement. Thus, for the high relative translational energies considered in this study, the HC stretch and HCH deformation modes are spectators and not coupled to the reaction coordinate. Initial rotational energies were chosen by sampling the components of angular momentum for CH_3Cl from a Boltzmann distribution at 300 K.

The trajectories were computed by solving Hamiltons equations of motion with combined fourth-order Runge−Kutta−Gill and sixth-order Adams−Moulton predictor corrector algorithms. The integration step size was chosen as 1.0×10^{-16} s (0.1 fs). This ensured energy conservation to five digits over the total integration time. Integration with a step size of 0.05 fs did not improve energy conservation or produce differences in the observed dynamics. The initial and final $Cl + CH_3Cl$ separations were chosen as 30.0 Å. For the 300 K CH_3Cl temperature and high values of E_{rel} considered here, these separations are of sufficient distance to give accurate results.

However, for lower E_{rel} and/or CH_3Cl temperature, larger separations may be necessary.[5b]

The attributes for reaction 2 determined from the trajectories include the reactive cross section, product energy and velocity scattering angle distributions, and angular momentum correlations. A total of 1000 trajectories were evaluated for each value of E_{rel}. The reactive cross section is given by

$$\sigma(E_{rel}) = \langle P_r(E_{rel})\rangle \pi b_{max}^2 \quad (7)$$

where $\langle P_r(E_{rel})\rangle$ is the average reaction probability with the impact parameter b chosen randomly between 0 and b_{max}. (The determination of b_{max} is discussed in the next section.) The velocity scattering angle is given by

$$\cos\theta = \mathbf{v}_i \cdot \mathbf{v}_f / |\mathbf{v}_i||\mathbf{v}_f| \quad (8)$$

where $\mathbf{v}_i$ and $\mathbf{v}_f$ are the initial and final relative velocity vectors, respectively. The energy available to the products E' is

$$E' = E_{rel}' + E_{int}' = E_{rel}' + E_{vib}' + E_{rot}' \quad (9)$$

The $ClCH_3$ internal energy E_{int}' is assumed separable into vibrational and rotational components. E_{rot}' is an average rotational energy calculated over the longest vibrational period τ of the product molecule, i.e.

$$E_{rot}' = \int_0^\tau E_{rot}(\tau)\, d\tau / \int_0^\tau d\tau \quad (10)$$

The instantaneous rotational energy $E_{rot}(\tau)$ is found from

$$E_{rot} = \boldsymbol{\omega} \cdot \mathbf{j}/2 \quad (11)$$

IV. Trajectory Results

A. Maximum Impact Parameter. A value of b_{max} for each E_{rel} was found by incrementing b by 0.25 Å until no reaction occurred out of 200 trajectories. The resulting reaction probability versus b, i.e., $P_r(b)$, was fit to find b_{max}. The values for b_{max} chosen in this manner are accurate to within 0.25 Å and are 1.70, 2.15, 2.23, 2.27, 2.40, 2.42, and 2.56 Å for E_{rel} of 20, 30, 40, 50, 60, 70, and 80 kcal/mol, respectively.

A dynamical model, which considers the rotational energy at the $[Cl\text{- -}CH_3\text{- -}Cl]^-$ central barrier, may be used to identify limiting values for b_{max}. At $T = 300$ K the average rotational angular momentum for CH_3Cl is $j \sim (2IRT)^{1/2} = 21.7\hbar$, where I is the largest moment of inertia for CH_3Cl. This angular momentum is much smaller than the $Cl^- + CH_3Cl$ orbital angular momentum $l = \mu b_{max} v_{rel}$, which ranges from $160\hbar$ to $481\hbar$ for the 20−80 kcal/mol range of E_{rel} values considered here. Thus, the total angular momentum for the $Cl^- + CH_3Cl$ system is well approximated by l.

For CH_3Cl with a 300 K vibrational/rotational energy distribution, the average classical energy available for rotation and vibration at the central barrier is $E^\ddagger = E_{rel} + {}^3/_2RT + E_{zp} - E_0$, where ${}^3/_2RT$ is the CH_3Cl average rotational energy, E_{zp} is the zero-point energy for the CH_3 umbrella and C−Cl stretch modes (at 300 K there is no significant population of these modes), and E_0 is the classical barrier height. The value for b_{max} is found by assuming all of $E^\ddagger$ becomes rotational energy (i.e., the trajectories are not vibrationally adiabatic and, thus, do not maintain zero-point energy at the barrier) and that l adds to the barrier's two rotational axes with the larger moment of inertia of $I^\ddagger = 411.03$ amu Å^2. Thus, b_{max} becomes

$$b_{max} = (I^\ddagger E^\ddagger / \mu E_{rel})^{1/2} \quad (12)$$

TABLE 3: Trajectory Cross Sections

E_{rel} (kcal/mol)	cross section (Å)[a]	E_{rel} (kcal/mol)	cross section (Å)[a]
20	0.027 ± 0.016	60	1.05 ± 0.13
30	0.22 ± 0.06	70	1.47 ± 0.16
40	0.37 ± 0.08	80	1.61 ± 0.17
50	0.83 ± 0.11		

[a] Uncertainties are for one standard deviation.

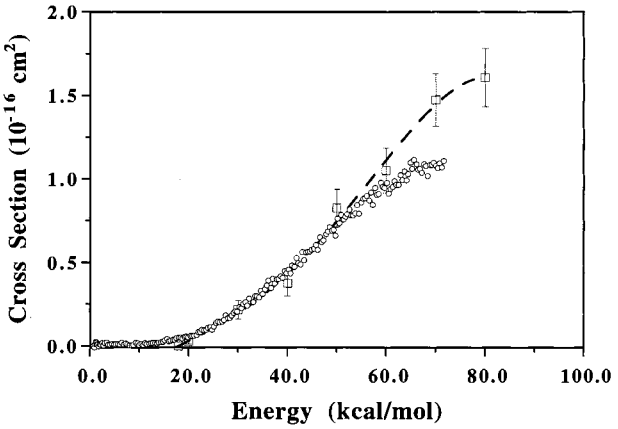

Figure 1. Trajectory (□) and experimental (○)[1i] reactive cross sections for reaction 2 versus E_{rel}. The experimental cross sections are arbitrarily scaled upward by a factor of 12.[11] The solid line is a fit to the trajectory data with a fourth-order polynomial. Uncertainties are for one standard deviation.

The resulting values of b_{max} are 3.99, 4.13, 4.20, 4.24, 4.27, 4.29, and 4.30 Å for E_{rel} of 20, 30, 40, 50, 60, 70, and 80 kcal/mol and are larger than the values found from the trajectories. The values are most similar at the highest E_{rel}, for which the trajectory b_{max} is 2.56 ± 0.25 Å.

B. Nature of the Trajectories. An important finding of this study is that only a very small fraction of the reactive and unreactive trajectories are indirect, with trapping in the ion−dipole wells. Of the 307 reactive trajectories, observed in the simulations, only one at both E_{rel} of 20 and 30 kcal/mol was temporarily trapped in one or both of the wells. No central barrier recrossing was observed in these trajectories.

Among the unreactive trajectories, only two out of 6693 were temporarily trapped in the Cl_a^-- - -CH_3Cl_b well, with multiple inner turning points in the relative center-of-mass motion. None of the unreactive trajectories accessed the Cl_aCH_3- - -Cl_b^- exit channel well. The small fraction of trapping results from the inefficiency of the system to transfer the initial E_{rel} to CH_3Cl_b rotational and vibrational modes.

C. Cross Sections and Translational Energy Threshold. Ervin and co-workers measured cross sections for reaction 2 up to a relative translational energy of 3 eV (69 kcal/mol). Here, cross sections were calculated for E_{rel} between 20 and 80 kcal/mol. The calculated cross sections range from 0.027 ± 0.016 to 1.61 ± 0.17 Å^2 and listed in Table 3. The trajectory and experimental cross sections are compared in Figure 1, where the latter values are scaled upward by a factor of 12 to match the trajectory magnitudes.[11] The shapes of the two cross-section curves are similar. The order of magnitude difference in the two sets of cross sections is discussed in the concluding section. The reactive cross section at E_{rel} of 50.0 kcal/mol and CH_3Cl temperature of 0 K was calculated previously[5a] using the potential energy surface PES1 for reaction 2. The resulting value is 0.28 ± 0.09 Å^2 and somewhat smaller than the value of 0.83 ± 0.11 Å^2 found here for PES3 at the same E_{rel}.

A frequently used method of determining threshold energies is the empirical threshold law, given by

$$\sigma(E_{rel}) = C(E_{rel} - E_{th})^N/E_{rel} \quad (13)$$

where E_{rel} is the relative translational energy, E_{th} is the translational energy threshold, and C and N are both adjustable parameters. Ervin and co-workers[1i] used a modification of eq 13 by summing over the experimental vibrational and rotational energy levels of the reactants. They obtained an estimate of 11 ± 4 kcal/mol to E_{th}. Equation 13 is used here to estimate E_{th} from the trajectory data. Cross sections were fit to eq 13 using the Levenberg−Marquardt algorithm. A series of fits were performed in order to minimize χ^2, the sum of the squares of the residuals. Both full optimization and partial optimizations were performed, with full optimization giving the smallest value of χ^2. The full optimization gives $C = 0.056$, $N = 1.88$, and $E_{th} = 17.9$ kcal/mol. The trajectory data were also fit to various polynomials, with the best overall fit being to a fourth-order polynomial, which also gives a threshold energy of 17.9 kcal/mol. The fit to this polynomial is shown in Figure 1.

D. Product Energy Distributions. Product energy distributions were computed as a function of the initial reactant relative translational energy. When determining the energy partitioning, the zero-point energy corresponding to the sampled A_1 C−Cl stretch and A_1 CH_3 umbrella modes was first subtracted from the $ClCH_3$ product vibrational energy. This zero-point energy is 3.13 kcal/mol. Plots of the average fractions of energy partitioned to product relative translation, rotation, and vibration versus initial relative translational energy are given in Figure 2. Energy is predominantly partitioned to relative translation, with smaller and similar fractions of energy partitioned to vibration and rotation. The preference for energy partitioning to relative translation is akin to the finding from experiments for the $F^- + CH_3Cl \rightarrow FCH_3 + Cl^-$ reaction,[12] but different than that observed in studies of Cl^-- - -$CH_3Br \rightarrow ClCH_3 + Br^-$ unimolecular dissociation.[1d,2e,13] For this latter reaction, most of the available energy was partitioned to product vibration.[14] Possible reasons for these differences in product energy partitioning are discussed in the concluding section.

Distributions of the product energies are shown in Figure 3 for the calculations with E_{rel} of 40, 60, and 80 kcal/mol. It is seen that the distributions broaden with increase in E_{rel}.

E. Velocity Scattering Angle Distribution. The distribution of the scattering angle θ between the initial and final relative velocity vectors is shown in Figure 4 for E_{rel} of 40, 60, and 80 kcal/mol. The initial velocity vector is defined as $\mathbf{v}_{Cl_a} - \mathbf{v}_{CH_3Cl_b}$ and the final velocity vector as $\mathbf{v}_{Cl_aCH_3} - \mathbf{v}_{Cl_b}$, so that scattering angles of 0 and π correspond to forward and backward scattering, respectively. There is significant broadening of the scattering angle distributions with increase in E_{rel}. Only backward scattering with $\theta > \pi/2$ is observed for E_{rel} of 60 kcal/mol and less. For higher values of E_{rel} there is a forward component to the scattering. The forward scattering trajectories occur for large initial impact parameters, which is indicative of a stripping mechanism. For $E_{rel} = 80$ kcal/mol forward scattering occurred for impact parameters in the range 2.1−2.5 Å. Smaller impact parameters resulted in backward scattering. Backward and forward scattering trajectories are depicted in Figure 5. In comparing the energy and velocity scattering angle distributions in Figures 3 and 4, it is seen that the rebound and stripping mechanisms are consistent with low and high product rotational energy, respectively.

F. Angular Momentum Correlations. The trajectories were analyzed to determine whether there are correlations between the components of the initial and final angular momenta. At low values of E_{rel} the initial orbital angular momentum l_i is transferred to product orbital angular momentum l_f, with a correlation coefficient of 0.95 at E_{rel} of 40 kcal/mol. This correlation is shown in Figure 6a. As E_{rel} is increased, this correlation begins to deteriorate; e.g., the (l_i,l_f) correlation coefficient is 0.85 and 0.81 at E_{rel} of 60 and 80 kcal/mol, respectively. The plot of l_i versus l_f at $E_{rel} = 80$ kcal/mol is shown in Figure 6b. The deterioration of the (l_i,l_f) correlation, with increase in E_{rel}, is consistent with the broadening of the product rotational energy distribution as E_{rel} is increased; i.e., see Figure 3c. The deterioration of this correlation probably arises from the onset of the stripping mechanism as E_{rel} is increased.

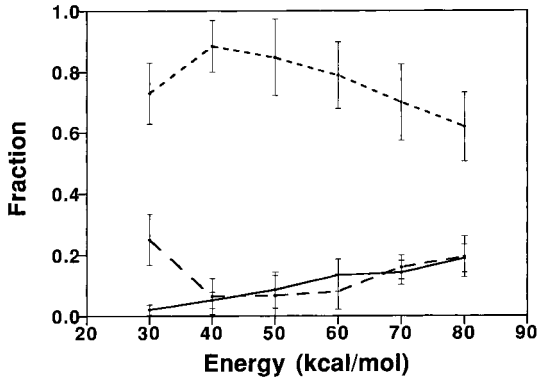

Figure 2. Average fraction of product relative translational (- - -), rotational (—), and vibrational (— —) energy versus E_{rel} in kcal/mol. Uncertainties are for a 95% confidence interval.

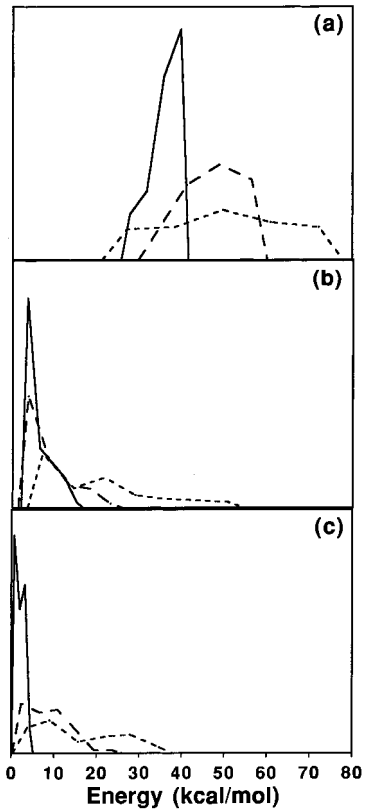

Figure 3. Distributions of product relative translational (a), vibrational (b), and rotational (c) energies for E_{rel} of 40 (—), 60 (— —), and 80 kcal/mol (- - -).

G. Kinetic Isotope Effect. For a fixed value of E_{rel}, Ervin and co-workers[1i] found that the reactive cross section for $Cl^- + CD_3Cl$ is smaller than that for $Cl^- + CH_3Cl$. To compare with this result, a trajectory reactive cross section was calculated for $Cl^- + CD_3Cl$ at $E_{rel} = 70$ kcal/mol. The resulting value is 1.21 ± 0.13 Å^2, compared to the value of 1.47 ± 0.16 Å^2 for

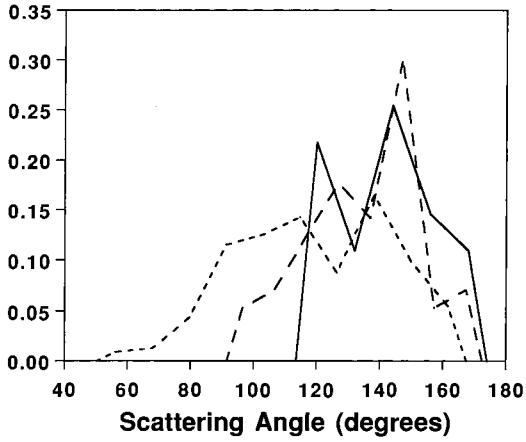

Figure 4. Distributions of the velocity scattering angle for E_{rel} of 40 (—), 60 (— —), and 80 (- - -) kcal/mol.

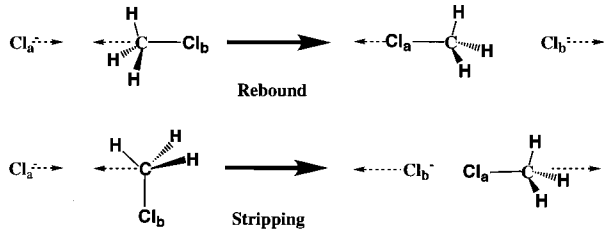

Figure 5. Depictions of backward and forward scattering trajectories.

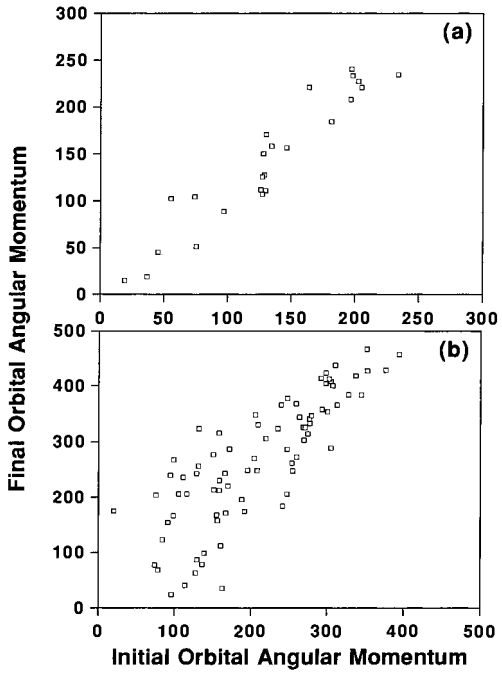

Figure 6. Scatter plots of the initial and final orbital angular momenta l_i and l_f; E_{rel} is 40 and 80 kcal/mol in (a) and (b), respectively. Angular momentum is in units of $\hbar$.

$Cl^- + CH_3Cl$. For the experiments at $E_{rel} = 70$ kcal/mol, the $Cl^- + CH_3Cl$ cross section is 1.16 times larger than that for $Cl^- + CD_3Cl$. The trajectory cross sections are consistent with this ratio.

The finding of an isotope effect from the trajectories, similar to that found in the experiments, appears to rule out tunneling as an explanation[1i] for the isotope effect. The origin of the isotope effect will require additional calculations and analyses. One possibility is that it is related to the CH_3:CD_3 umbrella frequency ratio, which is 1041:750 at the central barrier. It is

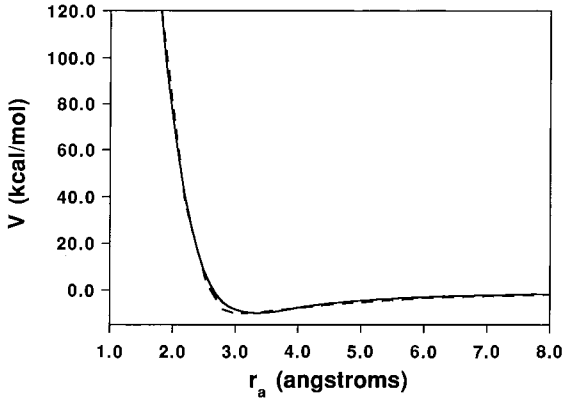

Figure 7. Comparison of PES3 (—) and MP2/6-311+G** (- - -) potential energies for Cl_a^- approaching CH_3Cl_b backside in a C_{3v} configuration, with the CH_3Cl_b geometry held fixed at the methyl chloride equilibrium geometry.

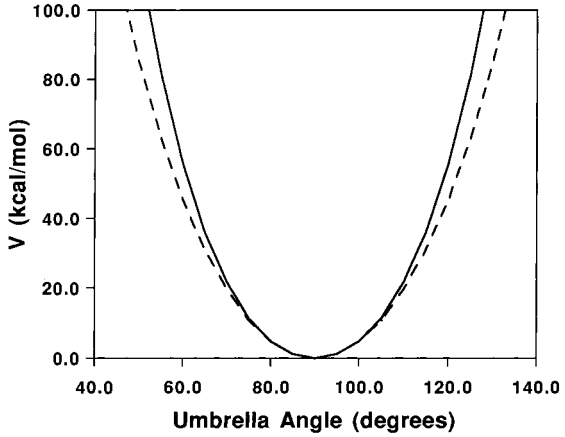

Figure 8. Comparison of PES3 (—) and MP2/6-311+G** (- - -) potential energies for deformation of the CH_3 umbrella angle at the central barrier, with the C—H and C—Cl bond lengths held fixed at their central barrier values.

of interest that the isotope effect found here for high E_{rel} is similar to that observed in previous trajectory studies of H + $CH_4(CD_4)$ substitution[15] and $CH_3(CD_3) + H_2$ abstraction,[16] also at high E_{rel}.

V. Accuracy of the PES3 Potential

As discussed above, though the change in the reactive cross section for reaction 2 versus E_{rel} calculated here is similar to the experimental results of Ervin and co-workers,[1i] the calculated cross sections are ~12 times larger. Since a possible origin for this difference could be inaccuracies in PES3, it was felt worthwhile to compare features of PES3 with those of a high-level ab initio calculation. The ab initio theory considered here is MP2/6-311+G**.[17] "Cuts" through regions of the potential energy surface, which are expected to have the greatest effects on the reactive cross section, are compared.

Figure 7 compares PES3 and MP2 potential curves for Cl_a^- approaching CH_3Cl_b backside in a C_{3v} configuration, with the CH_3Cl_b geometry held fixed at the methyl chloride equilibrium geometry. These curves address the repulsiveness of the potential energy surface when Cl_a^- collides backside in a Cl_a^-- - -C—Cl_b collinear geometry, without relaxation of the CH_3Cl_b moiety's structure. Figures 8—10 compare the PES3 and MP2 potential energy surfaces in the central barrier region. Figure 8 is a plot of the potential versus deformation of the CH_3 umbrella angle, with the C—H and C—Cl bond lengths

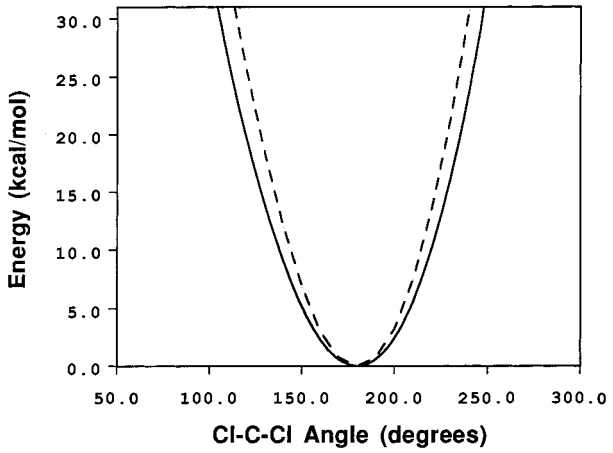

Figure 9. Comparison of PES3 (—) and MP2/6-311+G** (- - -) potential energies for bending the Cl−C−Cl angle at the central barrier (see text).

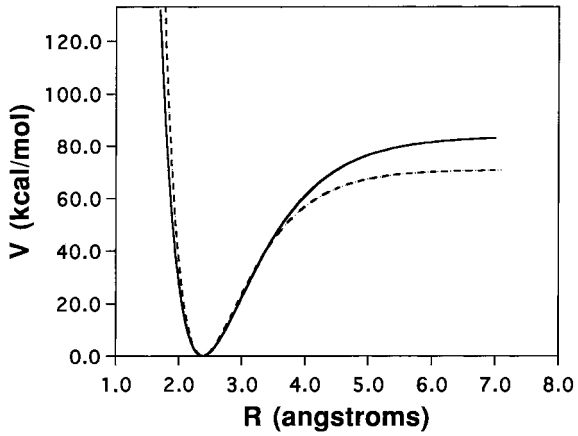

Figure 10. Comparison of PES3 (—) and MP2/6-311+G** (- - -) potential energies for symmetric Cl_a-C-Cl_b stretching at the central barrier; $R = (r_a + r_b)$. The energies are with respect to the central barrier potential, which is 3.5 and 8.1 kcal/mol for PES3 and the MP2 calculation, respectively. At large R the products are $Cl + CH_3 + Cl^-$.

fixed at their central barrier values. Figure 9 is a similar type plot, but instead of deforming the umbrella angle the Cl−C−Cl angle is bent by equal displacements of the Cl^- atoms in a plane containing a H atom of CH_3, while holding the structure of the CH_3 moiety and length of the C−Cl bonds fixed. Increase in the Cl−C−Cl angle corresponds to motion toward the H atom, while the motion is away from the H atom for decreases in the angle. Figure 10 is the potential energy curve for symmetric Cl_a-C-Cl_b bond stretching, and compression at the central barrier and is plotted versus $R = (r_a + r_b)$.

Figures 7−10 suggest there are no serious deficiencies in PES3. As shown in Figure 7, PES3 gives an overall good fit to the $Cl_a^- + CH_3Cl_b$ repulsive potential for symmetric collinear Cl_a^-- - - -$C-Cl_b$ backside collisions. Figures 8−10 illustrate important features of PES3 at the central barrier. Figure 8 shows that the deformation potential for the CH_3 umbrella angle at the central barrier is slightly more stiffer for PES3 than MP2, while Figure 9 shows that for the Cl−C−Cl bending potential the MP2 curve is slightly stiffer. For the latter and at a potential 30 kcal/mol in excess of the barrier height, the MP2 curve allows a 60°−65° closing of the Cl−C−Cl angle while a slightly larger closing of 70°−75° is allowed by the PES3 potential. The largest difference found here between the MP2 and PES3 potentials is for the symmetric $(r_a + r_b)$ potential energy curve at the central barrier. The MP2 curve for symmetric extension of $(r_a + r_b)$ has a 13 kcal/mol lower asymptotic value than does PES3. The PES3 curve is fit to the classical C−Cl dissociation energy of 87.4 kcal/mol.[18]

VI. Conclusion

The classical trajectory simulation reported here gives a translational energy dependence of the cross section for reaction 2 similar to that determined in recent experiments.[1i] The trajectory translational threshold is 18 kcal/mol and similar to the experimental value of 11 ± 4 kcal/mol. The trajectories also give a kinetic isotope effect consistent with the experiment. The principal difference between the trajectory and experimental studies is the order of magnitude larger trajectory reactive cross section. A careful comparison of PES3, the analytic potential energy function used in the trajectory study, and MP2/6-311+G** ab initio calculations showed no obvious deficiencies in PES3 that would make the trajectory reactive cross section an order of magnitude too large at high relative translational energies. This would arise from a maximum impact parameter b_{max} and/or opacity function $P_r(b)$ which is too large. In the future, it is important to further test and refine PES3 with additional high-level ab initio calculations.

The trajectories provide insight into the reaction dynamics which cannot be gleaned from the experiments. Translational activation is seen to give a direct reaction without trapping in the ion−dipole complexes. At low translational energies the trajectories display backward scattering and a rebound mechanism, while forward scattering and a stripping mechanism becomes increasingly important at higher translational energies. The total angular momentum is well-approximated by the initial orbital angular momentum, which is correlated with the final orbital angular momentum. This correlation becomes weaker as the reactant translational energy is increased, presumably because the stripping mechanism becomes more important.

The trajectories predict translational activation of reaction 2 gives translationally energized products, with much smaller amounts of energy partitioned to product vibration and rotation. This energy partitioning is distinctly different than that suggested from trajectory and experimental studies of Cl^-- - -$CH_3Br \rightarrow ClCH_3 + Br^-$ dissociation.[1d,2e,13] Here, energy is predominately partitioned to product vibration. There are important differences in the dynamics of these two systems which must be kept in mind when comparing their energy partitionings. The study reported here of reaction 2 involves translational activation and large total angular momentum. In contrast, the dissociation of Cl^-- - -CH_3Br is a vibrationally activated process, which occurs when energy is transferred into the rupturing C−Br bond. In addition, Cl^-- - -CH_3Br has a thermal total angular momentum, much lower than that for the translational activation of reaction 2.

The energy partitioning found here for the translational activation of reaction 2 is similar to that observed in thermal experiments[12] of the highly exothermic $F^- + CH_3Cl \rightarrow FCH_3Cl^-$ reaction.[19] This reaction has a very small central barrier[2g,20] and may occur without formation of the F^-- - -CH_3-Cl complex, followed by vibrational energy transfer to the C−Cl bond. The translational activation of reaction 2 and the $F^- + CH_3Cl$ reaction under thermal conditions may occur via similar microscopic mechanisms. Product energy partitioning in S_N2 reactions appears to be coupled to both the reaction under investigation and the way in which the reactants are energized.

It is of interest that three different elementary mechanisms have been identified for gas-phase S_N2 reactions. With reference to reaction 1, there is the original mechanism proposed by

Brauman and co-workers[21] in which a X^-- - -CH_3Y complex is formed first, followed by energy transfer to the C−Y bond to surmount the central barrier and then form products. Trajectory calculations for reaction 2 have also suggested a direct reaction for reactants with a thermal translational energy and vibrational activation of the C−Y bond.[3,5] This mechanism becomes more important for low CH_3 rotational energies, so that the incoming X^- ion can orient the CH_3Y dipole. Finally, the trajectory study reported here suggests a second direct mechanism, arising from translational activation of the reagents.

Acknowledgment. This research was supported by the National Science Foundation. The authors wish to thank Kent Ervin, Bob Continetti, Scott Anderson, Jim Farrar, and Cheuk Ng for very helpful discussions and Dr. Young June Cho for his help in deriving PES3.

References and Notes

(1) (a) Cyr, D. M.; Posey, L. A.; Bishea, G. A.; Han, C.-C.; Johnson, M. A. *J. Am. Chem. Soc.* **1991**, *113*, 9697. (b) Viggiano, A. A.; Morris, R. A.; Paschkewitz, X. X.; Paulson, J. F. *J. Am. Chem. Soc.* **1992**, *114*, 10477. (c) Knighton, W. B.; Bognar, J. A.; O'Connor, P. M.; Grimsrud, E. P. *J. Am. Chem. Soc.* **1993**, *115*, 12079. (d) Graul, S. T.; Bowers, M. T. *J. Am. Chem. Soc.* **1994**, *116*, 3875. (e) Li, C.; Ross, P.; Szulejko, J. E.; McMahon, T. B. *J. Am. Chem. Soc.* **1996**, *118*, 9360. (f) Craig, S. L.; Brauman, J. I. *J. Phys. Chem. A* **1997**, *101*, 4745. (g) Craig, S. L.; Brauman, J. I. *Science* **1997**, *276*, 1536. (h) Seeley, J. V.; Morris, R. A.; Viggiano, A. A.; Wang, H.; Hase, W. L. *J. Am. Chem. Soc.* **1997**, *119*, 577. (i) DeTuri, V. F.; Hintz, P. A.; Ervin, K. M. *J. Phys. Chem. A* **1997**, *101*, 5969. (j) LeGarrec, J.-L.; Rowe, B. R.; Queffelec, J. L.; Mitchell, J. B. A. *J. Chem. Phys.* **1997**, *107*, 1021. (k) Barlow, S. E.; Van Doren, J. M.; Bierbaum, V. M. *J. Am. Chem. Soc.* **1988**, *110*, 7240.

(2) (a) Peslherbe, G. H.; Wang, H.; Hase, W. L. *J. Chem. Phys.* **1995**, *102*, 5626. (b) Wang, H.; Hase, W. L. *J. Am. Chem. Soc.* **1995**, *117*, 9347. (c) Hu, W.-P.; Truhlar, D. G. *J. Am. Chem. Soc.* **1995**, *117*, 10726. (d) Glukhovtsev, M. N.; Pross, A.; Radom, L. *J. Am. Chem. Soc.* **1996**, *118*, 6273. (e) Peslherbe, G. H.; Wang, H.; Hase, W. L. *J. Am. Chem. Soc.* **1996**, *118*, 2257. (f) Wang, H.; Hase, W. L. *Chem. Phys.* **1996**, *212*, 247. (g) Wang, H.; Hase, W. L. *J. Am. Chem. Soc.* **1997**, *119*, 3093. (h) Clary, D. C.; Palma, J. *J. Chem. Phys.* **1997**, *106*, 575. (i) Wang, H.; Goldfield, E. M.; Hase, W. L. *J. Chem. Soc., Faraday Trans.* **1997**, *93*, 737. (j) Deng, L.; Branchadell, V.; Ziegler, T. *J. Am. Chem. Soc.* **1994**, *116*, 10645. (k) Glukhovtsev, M. N.; Pross, A.; Schlegel, H. B.; Bach, R. D.; Radom, L. *J. Am. Chem. Soc.* **1996**, *118*, 11258.

(3) Hase, W. L. *Science* **1994**, *266*, 998.

(4) Hase, W. L.; Wang, H.; Peslherbe, G. H. In *Advances in Gas-Phase Ion Chemistry*; Adams, N. G., Babcock, L. M., Eds.; JAI Press: Greenwich, CT, 1998; Vol. 3.

(5) (a) Vande Linde, S. R.; Hase, W. L. *J. Chem. Phys.* **1990**, *93*, 7962. (b) Hase, W. L.; Cho, Y.-J. *J. Chem. Phys.* **1993**, *98*, 8626.

(6) (a) Vande Linde, S. R.; Hase, W. L. *J. Phys. Chem.* **1990**, *94*, 2778. (b) Cho, Y.-J.; Vande Linde, S. R.; Hase, W. L. *J. Chem. Phys.* **1992**, *96*, 8275.

(7) Duncan, J. A.; Allan, A.; McKean, D. C. *Mol. Phys.* **1970**, *18*, 289.

(8) Hase, W. L.; Duchovic, R. J.; Hu, X.; Komornicki, A.; Lim, K. F.; Lu, D.-h.; Peslherbe, G. H.; Swamy, K. N.; Vande Linde, S. R.; Varandas, A.; Wang, H.; Wolf, R. J. *QCPE* **1996**, *16*, 671.

(9) Schatz, G. C. *J. Chem. Phys.* **1983**, *79*, 5386.

(10) Lu, D.-h.; Hase, W. L. *J. Chem. Phys.* **1989**, *91*, 7490. Miller, W. H.; Hase, W. L.; Darling, C. L. *J. Chem. Phys.* **1989**, *91*, 2863.

(11) DeTuri, V. F.; Ervin, K. M., private communication.

(12) VanOrden, S. L.; Pope, R. M.; Buckner, S. W. *Org. Mass Spectrom.* **1991**, *26*, 1003.

(13) Wang, H.; Peslherbe, G. H.; Hase, W. L. *J. Am. Chem. Soc.* **1994**, *116*, 9644.

(14) Direct $Cl^- + CH_3Cl$ S_N2 reaction, promoted by exciting the C−Cl stretch mode of CH_3Cl, results in preferential product energy partitioning to CH_3Cl vibration: Mann, D. J.; Hase, W. L., to be published.

(15) Valencich, T.; Bunker, D. L. *J. Chem. Phys.* **1974**, *61*, 21.

(16) Chapman, S.; Bunker, D. L. *J. Chem. Phys.* **1975**, *62*, 2890.

(17) Frisch, M. J.; Trucks, G. W.; Schlegel, H. B.; Gill, P. M. W.; Johnson, B. G.; Robb, M. A.; Cheeseman, J. R.; Keith, T.; Petersson, G. A.; Montgomery, J. A.; Raghavachari, K.; Al-Lahman, M. A.; Zakrzewski, V. G.; Ortiz, J. V.; Foresman, J. V.; Cioslowski, J.; Stefanov, B. B.; Nanayakkara, A.; Challacombe, M.; Peng, C. Y.; Ayala, P. Y.; Chen, W.; Wong, M. W.; Andres, J. L.; Replogle, E. S.; Gomperts, R.; Martin, R. L.; Fox, D. J.; Binkley, J. S.; Defrees, D. J.; Baker, J.; Stewart, J. P.; Head-Gordon, M.; Gonzalez, C.; Pople, J. A. *GAUSSIAN 94 Revision*; Gaussian, Inc.: Pittsburgh, PA, 1995.

(18) The classical C−Cl dissociation energy of 87.4 kcal/mol is determined from experimental heats of formation and vibrational frequencies; see ref 6.

(19) Trajectory studies for the $F^- + CH_3Cl \rightarrow FCH_3 + Cl^-$ reaction show that the product energy is preferentially partitioned to relative translation: Su, T.; Wang, H.; Hase, W. L. *J. Phys. Chem. A*, submitted.

(20) Botschwina, P.; Horn, M.; Seeger, S.; Oswald, R. *Ber. Bunsen-Ges. Phys. Chem.* **1997**, *101*, 387.

(21) Olmstead, W. N.; Brauman, J. I. *J. Am. Chem. Soc.* **1977**, *99*, 4219. Moylan, C. R.; Brauman, J. I. In *Advances in Classical Trajectory Methods*; Hase, W. L., Ed.; JAI Press: Greenwich, CT, 1994; Vol. 2.